



# Study on the influence of trains on the seismic response of high-speed railway structure under lateral uncertain earthquakes

Jian Yu<sup>1</sup> · Lizhong Jiang<sup>1,2</sup> · Wangbao Zhou<sup>1,2</sup>  · Jinyu Lu<sup>1</sup> · Tianxuan Zhong<sup>1</sup> · Kang Peng<sup>1</sup>

Received: 21 September 2020 / Accepted: 19 March 2021 / Published online: 25 March 2021  
© The Author(s), under exclusive licence to Springer Nature B.V. 2021

## Abstract

At present, specific earthquake motion is often used for analyzing the influence of trains on high-speed railway structure; however, the uncertainty of earthquake motion is rarely taken into consideration. In this study, on the basis of considering the uncertainty of earthquake motion, and taking a simply-supported beam with CRTS II track system and CRH2 high-speed train in China as the research objects, a finite element analysis model of vehicle-bridge coupled model was established and verified by tests. The influencing mechanism of the trains on structural response under the action of uncertain earthquake was analyzed, and the range of the influence levels of trains on seismic response of structure was calculated. The research findings show that under the effect of earthquake, the presence of trains decreases the responses of piers and bearings, while increases the response of track structure. With increasing peak ground acceleration, the effect of trains on the track structure deformation increases, while that on the bending moment of piers, shearing force, and bearing deformation all decrease. The increase in train speed will not significantly affect the seismic response of structures. The ratio of seismic response between the operating conditions with and without vehicles was kept within a certain range, so that the demand range for seismic response under the operating condition with vehicles can be approximately simplified.

**Keywords** Uncertain earthquake · Train · High-speed railway · Seismic response

---

Jian Yu and Lizhong Jiang have contribute equally to this paper.

---

✉ Wangbao Zhou  
zhouwangbao@163.com

<sup>1</sup> School of Civil Engineering, Central South University, Changsha 410075, China

<sup>2</sup> National Engineering Laboratory for High Speed Railway Construction, Changsha 410075, China

## 1 Introduction

In recent years, the construction of high-speed railway has been gradually extending to seismic fault zones in mountainous area and coastal areas with higher seismic intensity. There are more and more bridges, with increasingly wider span and deteriorating operating environment. Besides, the traffic density of high-speed trains is increasing, and there is a higher probability that high-speed railway structure is subjected to the joint action of trains and earthquakes. Therefore, studying the effect of high-speed trains on the structure's seismic response is valuable to ensure the safety of high-speed railway structure and has important theoretical significance and practical value in engineering.

Many researchers investigated the effect of train under the seismic action. Fan et al. (2014) studied the vibration of steel truss girder bridges under the joint action of trains and earthquakes, indicating that the trains decrease the peak values for lateral and vertical seismic acceleration of the bridge and increase the vibration frequency of structure. Zhang et al. (2011a, b) conducted seismic response analysis on high-speed railway bridges under the operating conditions with and without trains and pointed that the presence of trains would increase the lateral shear force acting on piers. Gao et al. (2020) studied the vehicle-bridge vibration of long-span continuous beams under vertical earthquake, indicating that the vertical displacement, velocity, and acceleration of the beam and the longitudinal bending moment of the pier all fluctuate with the train speed, reaching their maximum values at some specific train speed. Wang et al. (2011) calculated the lateral seismic response of bridge structure at different train speeds and pointed that the displacement of the pier top, the shear force, and bending moment of the pier showed significant nonlinear variation with varying train speed. Xia et al. (2006) studied the dynamic response of train-bridge system under the action of earthquake and pointed that the maximum lateral displacement and acceleration of the beam would vary with the train speed.

Researchers have conducted an in-depth analysis on the influencing mechanism of trains. Kim et al. (2007) studied the seismic response of monorail train, indicating that the monorail train on the bridge has the effect of shock absorption and energy dissipation on structure, because different natural vibration characteristics of train and bridge structure led to phase difference, thus reducing response of bridge. Therefore, considering the trains as an additional static mass rather than a dynamic system may lead to a relatively conservative result. He et al. (2011) studied the seismic response of vehicle-bridge on the Shinkansen and found that trains would reduce the seismic acceleration response of structure and verified the damping effects of trains on the structure under the action of earthquake. Gong et al. (2020) compared the vibration conditions of cable-stayed bridges when the trains pass at different speeds and pointed out that different train speeds would lead to different positions of trains on bridges, changing the vibration characteristics of the train-bridge system and affecting the vibration frequency and seismic response of the bridge and train body. Mu et al. (2016) studied the effects of track irregularity level and seismic load on the dynamic response of train-bridge system, indicating that track irregularity would significantly increase the dynamic response of train-bridge system. Xu and Zhai (2017) analyzed the random vibration of high-speed trains under the joint action of lateral earthquake motion and track irregularity excitation and found that track irregularity would aggravate the dynamic response of structure and increase the dispersion situation of seismic response. Zhang et al. (2010a, b, 2011a, b) compared the responses caused by track irregularity and earthquake excitation and pointed that the train speed had a significant effect on the vibration of bridge structure caused by track irregularity, but had only a slight

effect on the vibration caused by earthquake excitation. Zhang et al. (2010a, b) pointed that compared to track irregularity excitation, earthquake excitation contributed more to seismic response of structure.

The abovementioned literature reveals that the effect of trains on the seismic response of structure and the influencing mechanism are extensively investigated. However, they mainly considered specific earthquake motion for analyzing the effect of trains and rarely accounted the uncertainty of earthquake motion. Liu et al. (2018) compared the single-bridge model with train–bridge model and found that under the action of different earthquake motions, the effects of trains on the structure response show significant differences. He et al. (2011) pointed that the response of train–bridge interaction system is remarkably dependent on the frequency spectrum characteristics of earthquake motion, and the seismic response obtained through single earthquake motion lacked accuracy and representativeness; therefore, ignoring the uncertainty of earthquake motion might lead to an unreasonable influencing mechanism analysis. In addition, the abovementioned literature rarely clarified the influencing level range of trains on structural seismic response. The modeling process of train-track-bridge interaction may be overly complex for seismic design, and the determination of the influencing level range may help to simplify the train simulation (Yu et al. 2020).

Therefore, the main objective of this paper is to analyze the influencing mechanism and the influencing level range of trains on the structural response under the action of uncertain earthquake. In this study, through “magnitude-distance bin approach” (Tondini and Stojadinovic 2012), 100 earthquake motions with different characteristics were selected. Then, with the simply-supported beam with CRTS II track system and CRH2 high-speed train taken as the objects, the finite element model for train–bridge coupling was established and experimentally verified. The scientific significance of this paper is as follows: (a) an analysis was conducted on the influencing mechanism of trains on the structural response under the action of lateral uncertain earthquake. (b) The influencing level range of trains on structural response was statistically analyzed. (c) A simplified method was proposed for checking calculation on the seismic resistance of bridge structure.

## 2 Finite element analysis (FEA) model of high-speed railway system and its verification

### 2.1 FEA model of high-speed railway system

A 5-span simply-supported beam of 8-degree fortification with CRTS II slab ballastless track system was selected for analysis, as shown in Fig. 1. A standard prestressed concrete

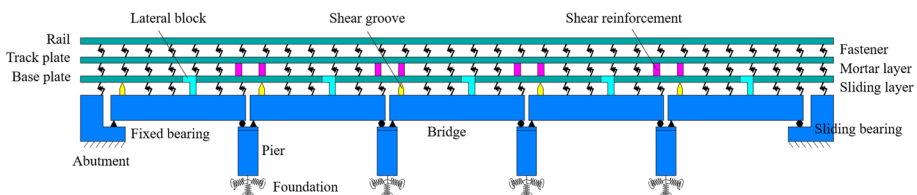


**Fig. 1** Schematic diagram of the high-speed railway system

box girder with a span of 32.5 m was used as the beam; round-ended solid piers with a height of 14 m were used as the piers; a seismic-resistant pot-type rubber bearing with a vertical bearing capacity of 5000 kN was used as the bearing. The dimensions of the base plate and track plate were  $2.95 \times 0.19 \text{ m}^2$  and  $2.55 \times 0.2 \text{ m}^2$ , respectively. The sliding layer with a thickness of 6 mm and the CA mortar layer with a thickness of 3 cm were paved between the base plate and box girder, and between the track plate and base plate, respectively. CHN60 rail was used as the rail and the fastener type is WJ-8C. Shear grooves were laid out on the beam surface above the fixed bearing, and a shear reinforcement was laid out between the track plate and base plate on both sides of the beam end, with lateral stop blocks laid out with a spacing of 5.74 m. The schematic diagram of each prototype structure is shown in Fig. 2.

A finite element model was established through ANSYS program. The box girder, pier, base plate, track plate, and rail were simulated by elastic beam elements, with the element length taken as a fastener spacing of 0.65 m; the sliding layer, CA mortar layer,

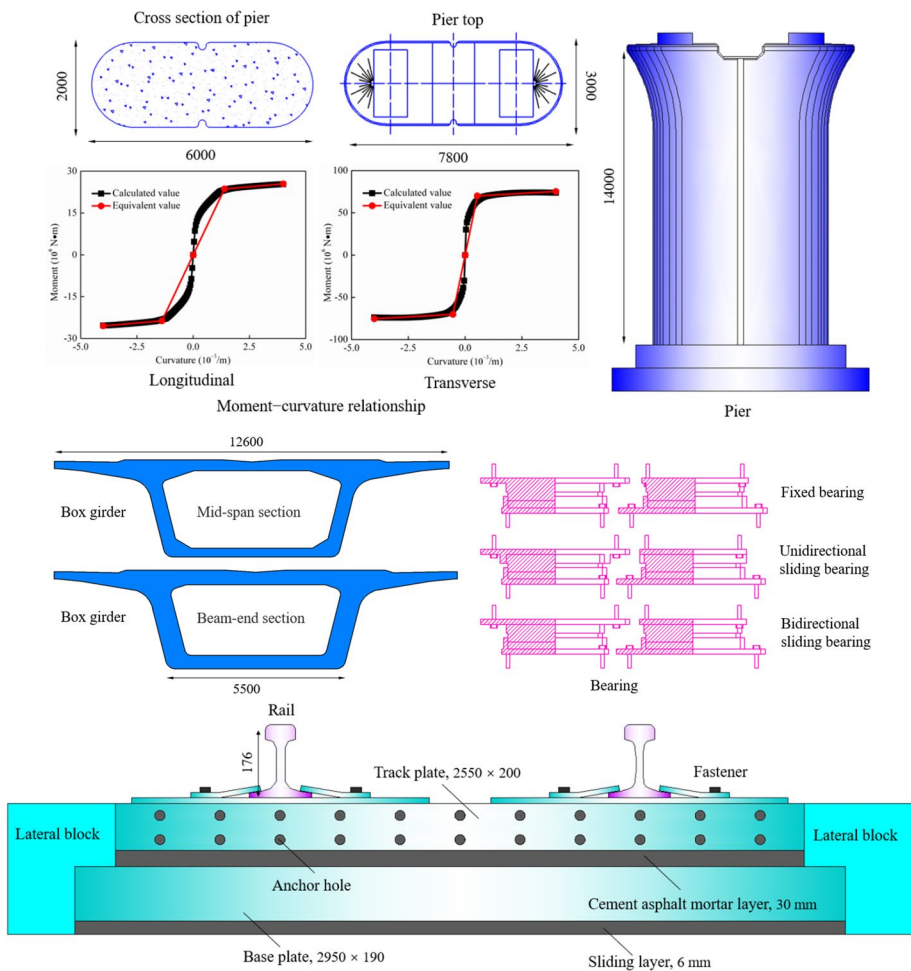


Fig. 2 Structural diagram of high-speed railway system (dimensions in mm)

fastener, bearing, shear groove, shear reinforcement and lateral block were simulated with nonlinear spring elements, and the force–displacement curves of the spring elements are listed in Table 1 (Feng et al. 2020; Jiang et al. 2020; Kang et al. 2017; Wei et al. 2018; Yan et al. 2017). The elasto–plastic deformation at the base of the pier was simulated by moment–curvature relationships (Fig. 2). The interaction between the pile and soil was simulated by spring elements. Rayleigh damping was adopted for the bridge with a damping ratio of 5%. The time step of seismic analysis was 0.01 s. The equation solver, convergence criterion and iteration accuracy were set as default.

### 2.2 Train model

The model of the high-speed railway train was CRH2C train, and the main parameters of the train are shown in Table 2 (Zhai et al. 2015). The selected train is composed of 2 power carriages and 14 passenger carriages. Each carriage was simulated as 8 mass springs with the central line at the wheel set, with  $M_v$ ,  $M_b$ ,  $M_w$ ,  $K_1$ ,  $K_2$ ,  $C_1$  and  $C_2$  as well as  $m_v$ ,  $m_b$ ,  $m_w$ ,  $k_1$ ,  $k_2$ ,  $c_1$  and  $c_2$  denoting the vehicle body mass, bogie mass, wheel set mass, primary spring stiffness, secondary spring stiffness, primary spring damping and secondary spring damping of each carriage and those distributed on each mass spring, respectively. Rigid bars were used to connect  $m_v$ ,  $m_b$  and  $m_w$  on the two rails, as shown in Fig. 3. According to equivalence principle (Chen et al. 2014), the above physical quantities satisfy the following corresponding relationship:  $M_v = 8m_v$ ,  $M_b = 4m_b$ ,  $M_w = 2m_w$ ,  $K_1 = k_1$ ,  $K_2 = 2k_2$ ,  $C_1 = c_1$  and  $C_2 = 2c_2$ .

In this study, the contact points between the wheel set and rail were assumed to have the same lateral and vertical freedom degrees. The feasibility of this method has been verified by several literature reports (He et al. 2011; Kim and Kawatani 2006; Kim et al. 2007; Lee et al. 2005; Yu et al. 2020). For example, He et al. (2011) found that the structure response calculated through this method coincided well with the experimental data. Lee et al. (2005) used the field test and verified that the simulation method had enough calculation accuracy for the structure.

**Table 1** The force–displacement curves of the spring elements

Force–displacement curve	Component	$F_y/kN$	$F_x/kN$	$D_y/mm$	$D_x/mm$
	Shear groove	1465	1465	0.12	0.12
	Fixed bearing	1000	1000	2.00	2.00
	Sliding bearing	100	100	2.00	2.00
	Lateral block	453	0	2.00	0.00
	CA mortar layer	42	42	0.50	0.50
	Fastener	24	9	2.00	2.00
	Shear reinforcement	23	23	0.08	0.08

**Table 2** Main parameters of the CRH2C train

Property	Value	Unit
Distance between bogie centres	2.5	m
Bogie wheelbase	17.5	m
Car body mass	35,000	kg
Bogie frame mass	3300	kg
Wheelset mass	1800	kg
Primary (per axle box) and secondary (per side of bogie) suspension longitudinal stiffness	14,680 and 160	kN/m
Primary (per axle box) and secondary (per side of bogie) suspension lateral stiffness	6470 and 160	kN/m
Primary (per axle box) and secondary (per side of bogie) suspension vertical stiffness	1176 and 190	kN/m
Primary (per axle box) and secondary (per side of bogie) suspension longitudinal damping coefficient	0 and 5.06	kN·s/m
Primary (per axle box) and secondary (per side of bogie) suspension lateral damping coefficient	0 and 58.86	kN·s/m
Primary (per axle box) and secondary (per side of bogie) suspension vertical damping coefficient	5 and 39.87	kN·s/m

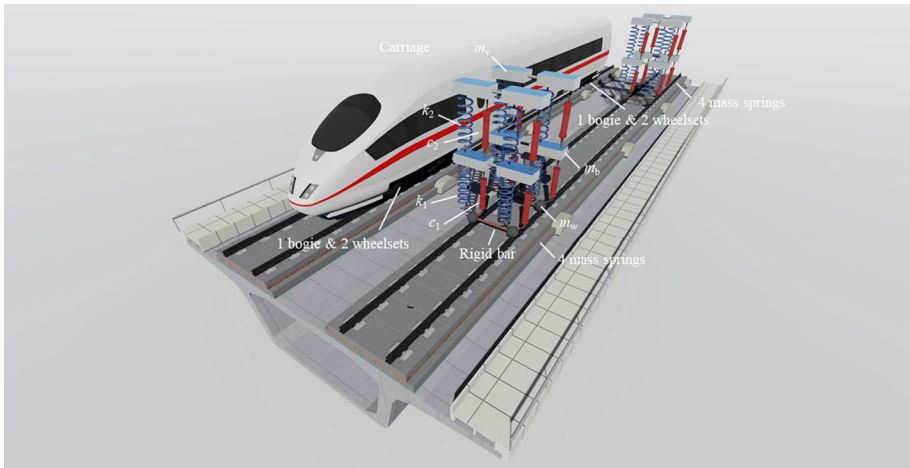


**Fig. 3** Train model and equivalent mass springs

The train-track-bridge coupling vibration under earthquake action was achieved using ANSYS program through the following steps: (1) judging the spatial position of each mass spring according to the moving speed of the train, applying longitudinal displacement constraint to it and coupling the vertical and lateral freedom degrees of the nodes between the moving wheelset and rail; (2) earthquake was used as input acceleration to solve the dynamic response of structure; (3) at the next time point, all the couplings were removed and Step (1) was repeated. Assuming that earthquake motion was instantly applied at the moment when the first carriage left the bridge, and enough carriages were arranged to ensure the travel time of the train on the bridge was longer than the action time of earthquake motion.

### 2.3 Model verification

To verify the validity of the finite element model, driving test was carried out under the lateral earthquake. The whole testing system comprises a shaking table system, a scale model, and acceleration and deceleration devices of the train, a transition device, and a measuring system, as shown in Fig. 4.

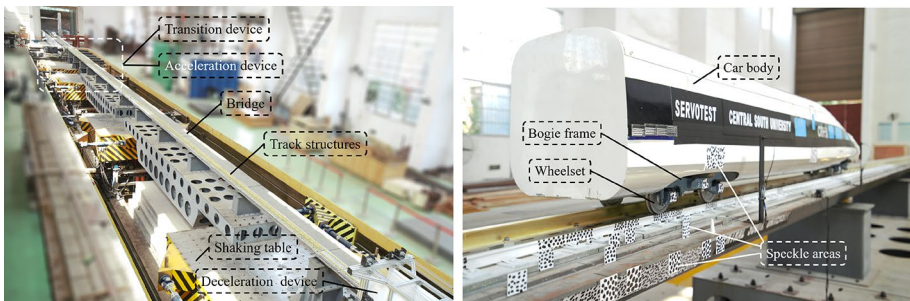


**Fig. 4** The shaking table system and the scaled bridge-track-train model



The shaking table system comprises four shaking tables with a dimension of 4 m × 4 m. The maximum length in the working area of the shaking table system is 55 m, which is suitable for seismic-resistant test on the bridge structure.

To ensure enough observation time, the span number of the scaled bridge model was set to be 11, and the geometric similarity ratio  $S_L$  was set to be 1/10. To avoid the effect of gravity distortion on the response of vehicle-bridge system, the acceleration similarity ratio  $S_a$  was taken as 1. The test specimen's mass is directly proportional to the material's similarity ratio  $S_E$ . To control the mass of the test specimen,  $S_E$  was set as 1/2. Other similarity coefficients (Fig. 5) were determined by dimensional analysis method (Jiang et al. 2019; Kang et al. 2017). The box girder, base plate, pier, track plate, rail, and other structures of the scale model were designed according to the principle of equivalent bending stiffness; the structures such as bearing, sliding layer, CA mortar layer, and fastener were designed according to the principle of equivalent resistance force; the shear reinforcement, shear groove, and lateral stop block were designed to be strong enough because they tend to remain intact during earthquakes (Feng et al. 2020), with the test specimen shown in Fig. 5. The train model was customized by the factory according to the similarity ratio.

A VIC-3D high-speed camera system was used as the measuring system, with the maximum width of the observation area as about 2 m. The high-speed camera shooting frequency was set as 2000 FPS, and the measurement tolerance of displacement is within 0.01 mm. Considering that the track structure near beam end was more likely to be subjected to deformation and failure under the action of earthquake, the observation areas were arranged between #5 box girder and #6 box girder, with the measuring arrangement shown in Fig. 6. The artificial wave synthesized from the site response spectra was used as the seismic excitation in the test, as shown in Fig. 7.

At the beginning of the test, the model train was accelerated to the test speed (5 m/s) in the acceleration area and entered the bridge model through the transition device. At the moment when the train got on the bridge, the transition device was disconnected immediately; the testing system started recording and the shaking table started generating the seismic excitation until the train left the bridge and entered the deceleration zone. The

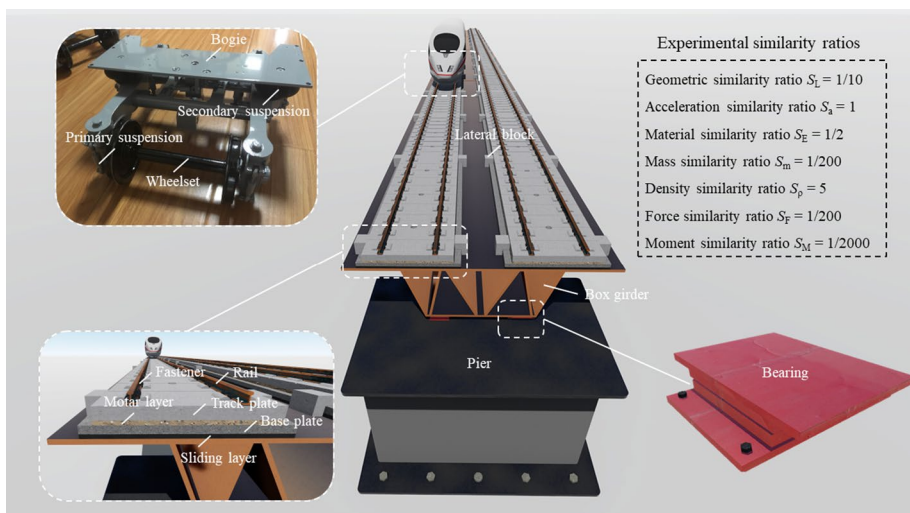
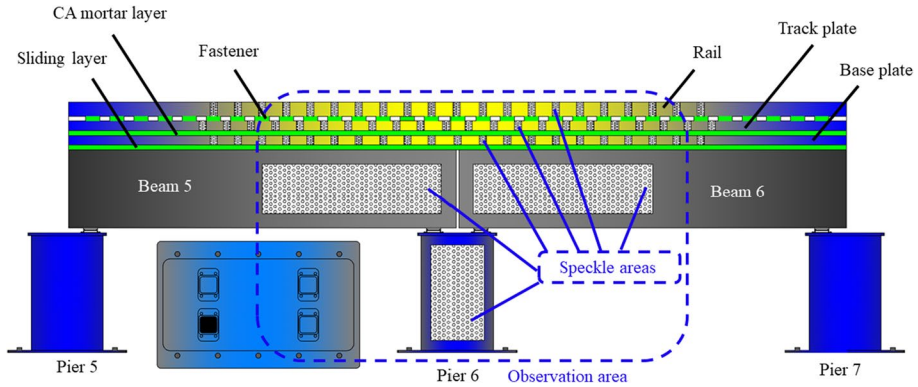
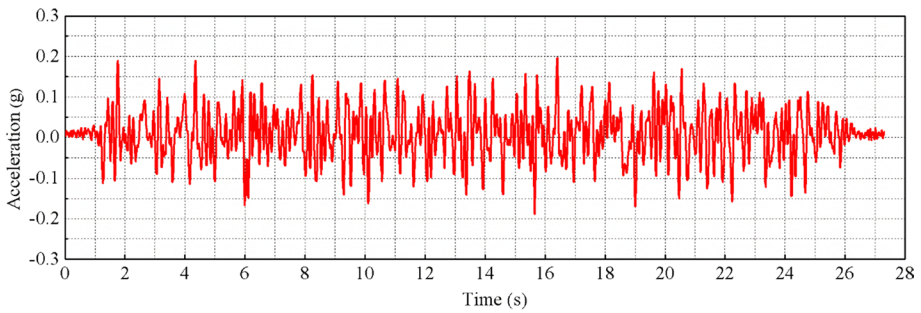


Fig. 5 Schematic diagram of the specimens





**Fig. 6** Arrangement of speckle areas and acceleration sensors



**Fig. 7** Lateral acceleration time history of the prototype

measured data on the measuring points within the beam end area were compared to the data provided by the finite element model, with the results shown in Fig. 8 and Table 3. The numerical calculation results for lateral displacement and acceleration of the structure coincided well with the measured values, with the maximum deformation error of components ranging between 9 and 17%. This indicated that the finite element model could accurately simulate the structural vibration under the action of earthquake and could be used to study the effect of trains on the seismic response of structures.

### 3 Analysis of the influencing mechanism of trains on seismic response of structures

#### 3.1 Earthquake motions

In this study, “magnitude-distance bin approach” (Tondini and Stojadinovic 2012) was used to select earthquake motions. The purpose of this method was to cover the random characteristics of earthquake motions by selecting the least earthquake motions. With  $M=6.5$  taken as the boundary between large and small earthquake magnitudes and  $R=30$  km as the boundary between near-field earthquake and far-field earthquake, four

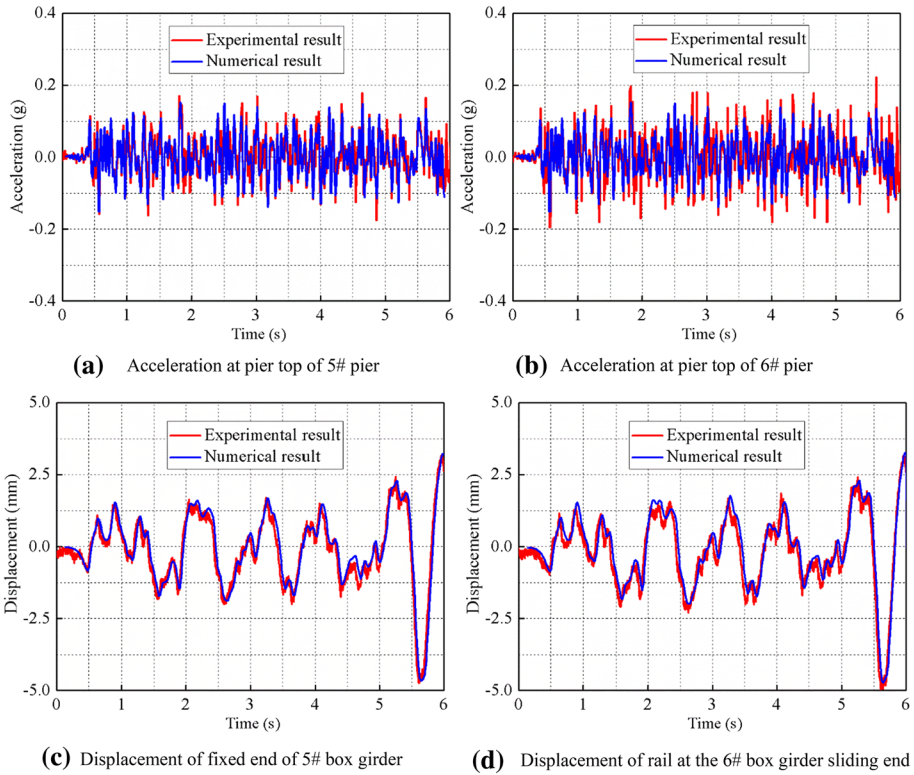


**Fig. 8** Lateral response of structure under the action of earthquake

**Table 3** The maximum deformation of components at the 6# box girder sliding end

Item	Test value (mm)	Numerical simulation (mm)	Error (%)
Deformation of fixed bearing	0.27	0.30	11
Deformation of sliding bearing	0.28	0.30	9
Deformation of sliding layer	0.31	0.26	16
Deformation of mortar layer	0.24	0.20	17
Deformation of rail fastener	0.32	0.28	13

earthquake motion bins with different characteristics were formed. 100 seismic waves were selected from the PEER strong earthquake database and evenly distributed to each bin, as shown in Table 4.

### 3.2 Effect of train presence on seismic response of structures

According to the possibility and intensity of earthquake occurrence, the seismic zones in China were divided into 6, 7, 8, and 9-degree fortification areas. The bridge site was located in an 8-degree fortification area, and the peak acceleration of the rare earthquake

**Table 4** Earthquake motion bins

Bin name	Magnitude range	Epicenter range (km)	Number of seismic waves
LMSR (large magnitude, small distance)	6.5–8	0–30	25
LMLR (large magnitude, large distance)	6.5–8	30–100	25
SMSR (small magnitude, small distance)	5–6.5	0–30	25
SMLR (small magnitude, large distance)	5–6.5	30–100	25

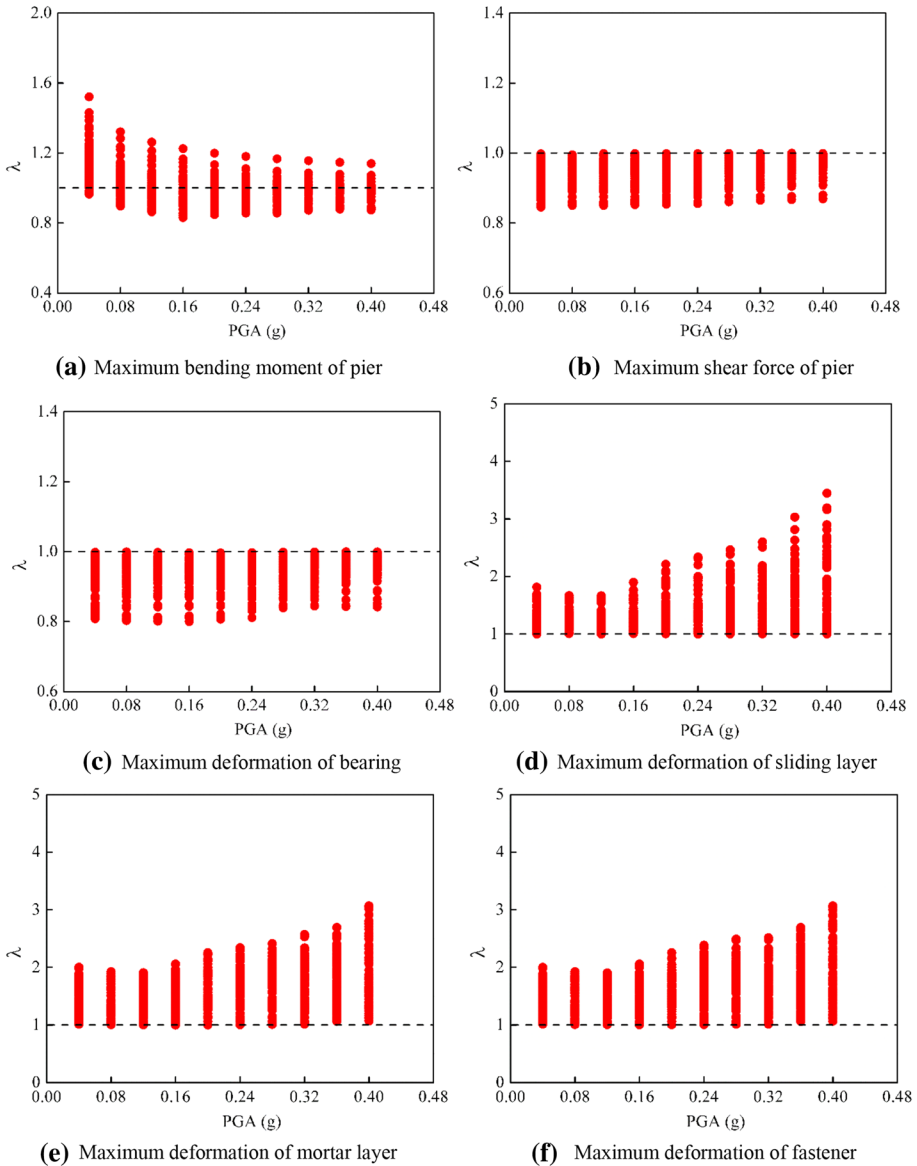
corresponding to the field was 0.38 g. To study the effect of train presence on the structural seismic response under different PGAs, the PGA of 100 earthquake motions was set to be from 0.04 to 0.4 g with an interval of 0.04 g; the operating conditions with and without train conditions were set. The train speed was set to be 300 km/h. The nonlinear time-history analysis was carried out for each operating condition, and the seismic response of structures was extracted. The maximum seismic response ratio of the structures under the operating conditions with and without trains was denoted as  $\lambda$ , indicating the effect level of trains on the seismic response of structures. The distribution of the scattered  $\lambda$  points is shown in Fig. 9.

Figure 9 shows that when PGA was 0.04 g, most scattered  $\lambda$  points corresponding to the maximum bending moment of pier were distributed above the dotted line ( $\lambda = 1$ ), indicating that when PGA was smaller, the eccentric effect caused by the train had a significant effect on the bending moment of the pier. With increasing PGA, the scattered  $\lambda$  points moved downward from the dotted line, indicating that the effect of eccentric effect caused by trains decreased with increasing PGA. The scattered  $\lambda$  points corresponding to the maximum shear force of the pier, the maximum deformations of the bearing, and the maximum deformation of the sliding layer, mortar layer and fastener were generally located below and above the dotted line, respectively. The comparison between the response time history of one earthquake motion with or without vehicles (as shown in Fig. 10) indicated that the presence of trains under the action of earthquake decreased the response of the bridge piers and bearing, while enhanced the response of the track structure, because the deformation (Fig. 11) of the train itself and the deformation of track structure caused by the train absorbed part of seismic energy.

The mean values of the scattered  $\lambda$  points are shown in Fig. 12, showing increasing trend regarding the maximum deformation of sliding layer, mortar layer, and fastener with increasing PGA, because the increase in PGA increased the acting force of the train on the track structure. The mean values of the scattered  $\lambda$  points regarding the maximum bending moment, maximum shear force of the pier, and the maximum deformation of bearing gradually tended to be 1, indicating that the proportion of seismic energy dissipation caused by the train decreased with increasing PGA, and most seismic energy still dissipated by the pier and bearing under the action of strong earthquake motion.

### 3.3 Effect of train speeds on seismic response of structures

To study the effect of train speeds on the structural seismic response, the train speeds were set to be from 50 to 300 km/h with an interval of 50 km/h. Twenty seismic waves were selected from the earthquake motion bins, and their peak accelerations were set to be from



**Fig. 9** Scattered point distribution of  $\lambda$  for lateral seismic response of structure

0.04 to 0.4 g with an interval of 0.04 g. The nonlinear time-history analysis was carried out, and the mean values of the scattered  $\lambda$  points under different speeds are shown in Fig. 13.

The mean values of the scattered  $\lambda$  points regarding the maximum bending moment, the maximum shear force of the pier, the maximum deformation of bearing, the maximum deformation of the sliding layer, mortar layer, and fastener did not show significant differences with changing train speed. The above results indicated that the change in the train speed would not significantly affect the seismic response of structures.

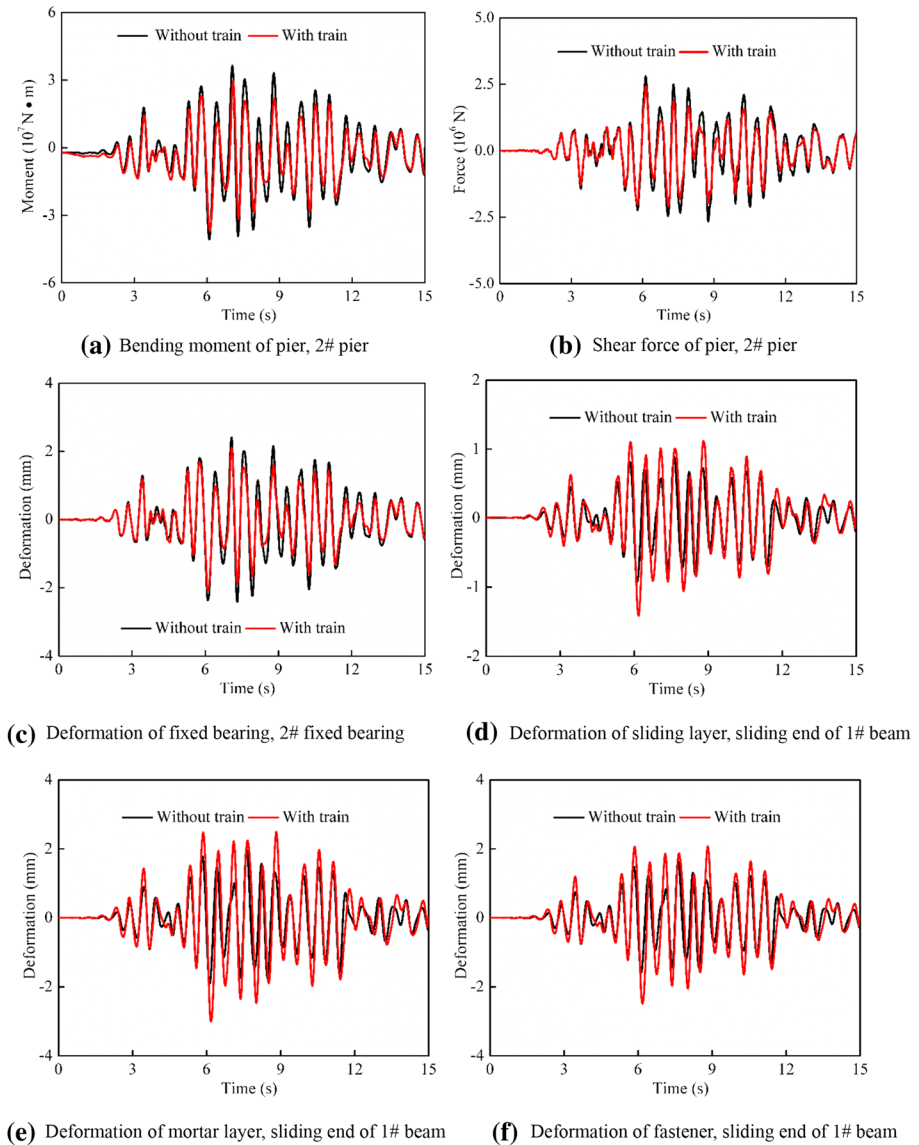
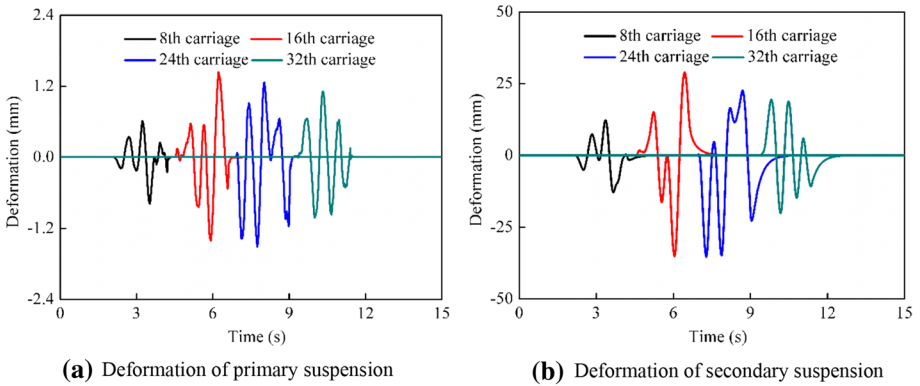


Fig. 10 Lateral seismic response of structure (Earthquake: Kobe, PGA = 0.2 g)

## 4 Range of influencing levels of trains on seismic response of structures

### 4.1 Range analysis method

The obtained scattered  $\lambda_i (i = 1, 2, \dots, k)$  points and all possible scattered  $\lambda_i (i = 1, 2, \dots, \infty)$  points are considered as samples and population, respectively. To study the range of influencing levels of trains on seismic response of structure, there are three issues that need to be



**Fig. 11** Lateral deformation of train (Earthquake: Kobe, PGA=0.2 g,  $v = 300$  km/h)

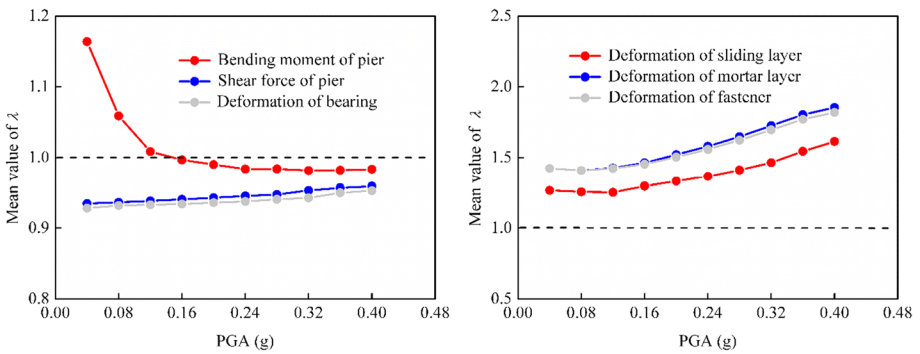


**Fig. 12** Mean value of  $\lambda$  for lateral seismic response of structure

addressed (Jiang et al. 2020): (a) what is the statistical distribution model of the population; (b) whether the samples represent the population; (c) how to predict the population. They are known as three basic tasks in statistics, which can be solved by Jarque–Bera test, Chebyshev’s large number theorem and parameter estimation principle, respectively. The flow chart of the range analysis method is shown in Fig. 14.

Assuming that the structure is subjected to  $k$  earthquakes, each index corresponds to a set of scattered points of  $\lambda_i (i = 1, 2, \dots, k)$ , and the scattered  $\lambda_i$  points are regarded as the random samples of the population  $\lambda$ . Sample skewness  $S$  and sample kurtosis  $K$  can be expressed as (Jarque 2011):

$$S = \frac{\frac{1}{k} \sum_{i=1}^k (\lambda_i - \bar{\lambda})^3}{\left(\frac{1}{k} \sum_{i=1}^k (\lambda_i - \bar{\lambda})^2\right)^{\frac{3}{2}}}, \quad K = \frac{\frac{1}{k} \sum_{i=1}^k (\lambda_i - \bar{\lambda})^4}{\left(\frac{1}{k} \sum_{i=1}^k (\lambda_i - \bar{\lambda})^2\right)^2} \tag{1}$$

where  $\bar{\lambda}$  denotes the mean value of  $\lambda_i$ . Statistics  $J_1$  and  $J_2$  are constructed as follows:

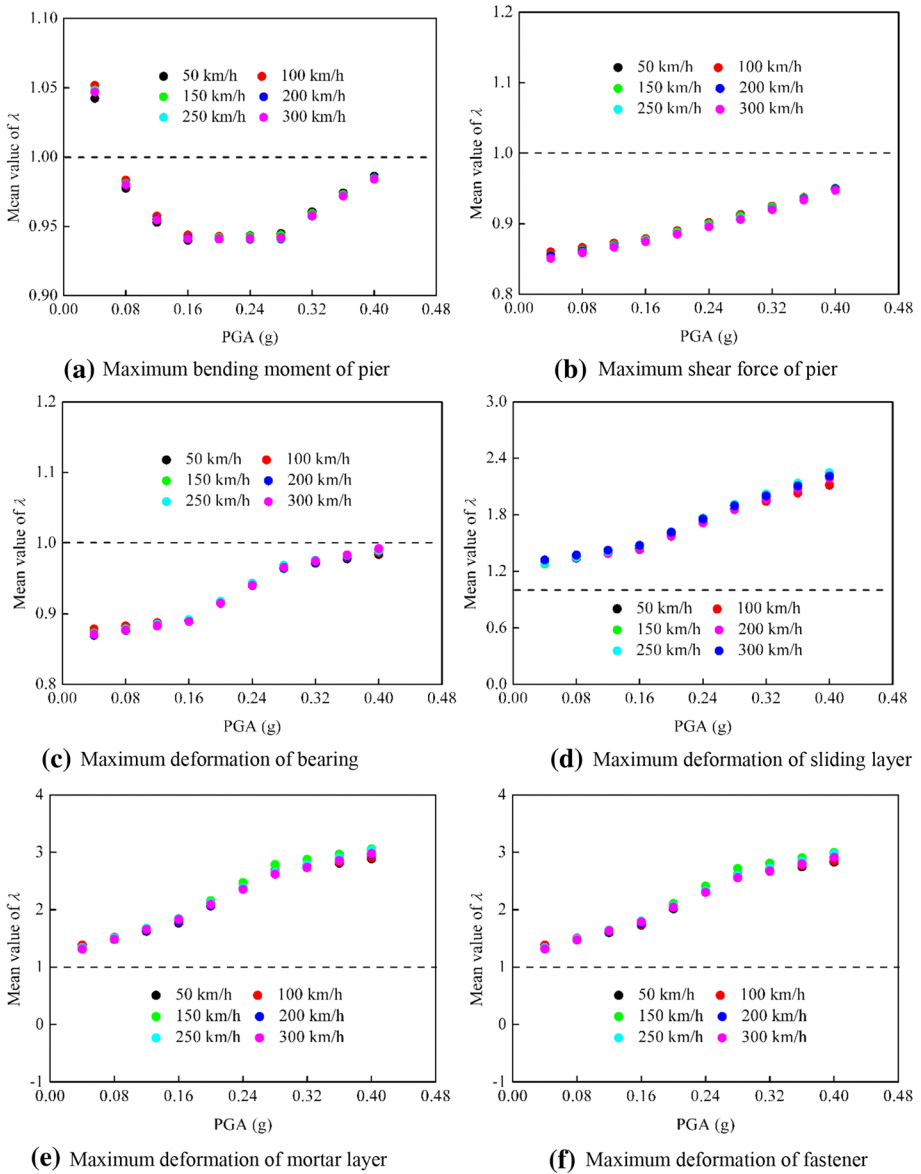


**Fig. 13** Mean value of  $\lambda$  for lateral seismic response of structure

$$J_1 = \frac{k}{6} \left( S^3 + \frac{(K-3)^2}{4} \right) - \chi^2(2), \quad J_2 = \begin{cases} 0, & J_1 < 0 \\ 1, & J_1 > 0 \end{cases} \quad (2)$$

where  $\chi^2$  denotes chi-square distribution. When  $J_2$  is 0, it indicates that the population  $\lambda$  meets the normal distribution, that is:

$$\lambda \sim N(\mu, \sigma^2) \quad (3)$$



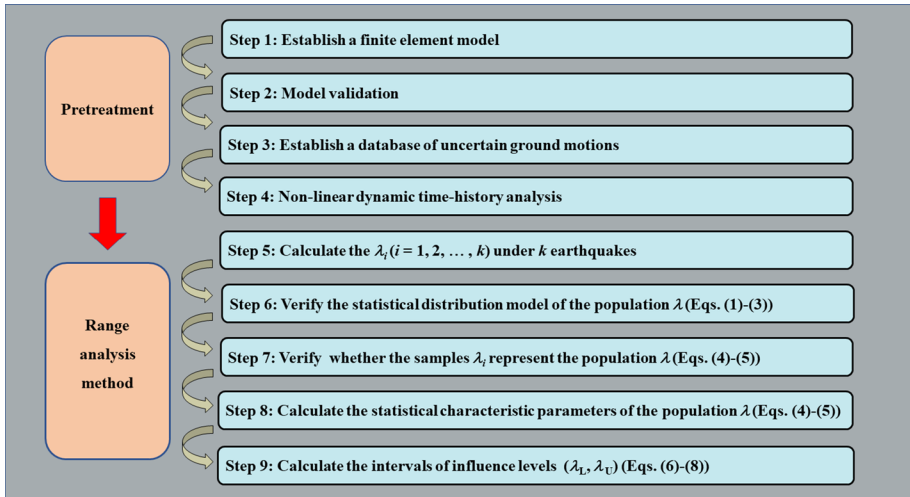


Fig. 14 Flow chart of the range analysis method

where  $\mu, \sigma^2$  denote the mean and variance of the population  $\lambda$ , respectively. The sample variance of  $\lambda_i$  is denoted as  $s^2$ . Chebyshev’s law of large numbers led to the following equations:

$$\lim_{k \rightarrow \infty} \bar{\lambda} = \lim_{k \rightarrow \infty} \frac{1}{k} \sum_{i=1}^k \lambda_i = \mu \tag{4}$$

$$\lim_{k \rightarrow \infty} s^2 = \lim_{k \rightarrow \infty} \frac{1}{k-1} \sum_{i=1}^k (\lambda_i - \bar{\lambda})^2 = \sigma^2 \tag{5}$$

Equations (4) and (5) indicated that with increasing number of samples, the sample mean value and sample variance of  $\lambda_i$  would gradually converge to a certain constant. It could be held that  $\lambda_i$  and  $\lambda$  had the same statistical characteristics.

With the significance level denoted as  $\alpha$ , the lower boundary  $\lambda_L$  and upper boundary  $\lambda_U$  were introduced. For the population  $\lambda$ , the following equations were obtained:

$$P\{\lambda_L \leq \lambda \leq \lambda_U\} = 1 - \alpha \tag{6}$$

i.e.,

$$P\left\{\frac{\lambda_L - \bar{\lambda}}{s} \leq \frac{\lambda - \mu}{\sigma} = \frac{\lambda - \bar{\lambda}}{s} \leq \frac{\lambda_U - \bar{\lambda}}{s}\right\} = 1 - \alpha \tag{7}$$

To make Eq. (5) tenable,  $\lambda_L$  and  $\lambda_U$  should satisfy the following equation:

$$\lambda_L = Sz_{\frac{\alpha}{2}} + \bar{\lambda}, \lambda_U = Sz_{\frac{\alpha}{2}} + \bar{\lambda} \tag{8}$$

where  $z$  denotes the quantile on standard normal function. With the  $\alpha$  taken as 0.10, the intervals of influence levels ( $\lambda_L, \lambda_U$ ) can be calculated.

**Table 5**  $J_2$  of the scattered  $\lambda_i$  points corresponding to different PGA

Category	PGA (g)									
	0.04	0.08	0.12	0.16	0.20	0.24	0.28	0.32	0.36	0.40
Maximum bending moment of pier	0	0	0	0	0	0	0	0	0	0
Maximum shear force of pier	0	0	0	0	0	0	0	0	0	0
Maximum deformation of bearing	0	0	0	0	0	0	0	0	0	0
Maximum deformation of sliding layer	0	0	0	0	0	0	0	0	0	0
Maximum deformation of CA mortar layer	0	0	0	0	0	0	0	0	0	0
Maximum deformation of fastener	0	0	0	0	0	0	0	0	0	0

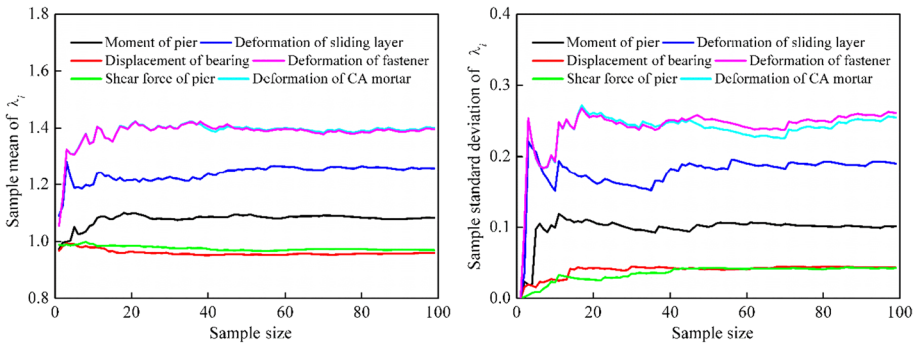


**Fig. 15** Sample mean and sample variance of  $\lambda_i$

### 4.2 Example analysis

The scattered  $\lambda_i (i = 1, 2, \dots, 100)$  points in Fig. 9 were extracted. Through the combination of Eqs. (1)–(3),  $J_2$  corresponding to different PGA was calculated (Table 5), and on each PGA the value of  $J_2$  was 0, indicating that the population  $\lambda$  obeyed normal distribution.

By taking  $PGA = 0.2 \text{ g}$  as an example, through the combination of Eqs. (4) and (5), the change of the sample mean and sample standard deviation for  $\lambda_i$  of each index with the number of samples was counted, as shown in Fig. 15. The differences in the sample mean and variance of  $\lambda_i$  and  $\lambda_{i-10}$  were denoted as  $\Delta\lambda_i$ , with  $\Delta\lambda_i$  corresponding to different sample sizes listed in Table 6. Figure 15 and Table 6 show that with the increase in  $k$ , the mean and standard deviation of the sample gradually tended to be stable, verifying the validity of Eqs. (4) and (5). When  $k$  was taken as 100, the  $\Delta\lambda_i$  of each index was within 1.3%, indicating that  $\lambda_i$  had a stable statistical property in this case. The statistical properties of the population  $\lambda$  can be denoted by the statistical property of  $\lambda_i$ , i.e.,  $\mu = \bar{\lambda}, \sigma = s$ . Therefore, in this study,  $\lambda_i (i = 1, 2, \dots, 100)$  was used to predict the distribution interval of  $\lambda$  under the action of uncertain earthquake.

With the  $\alpha$  taken as 0.10, through the combination of Eqs. (6)–(8),  $\lambda_L, \lambda_U$  and the intervals of influence levels were calculated and are shown in Table 7. Under the action of earthquake,  $\lambda$  for the bending moment of the pier and that for the track deformation reached 1.32 and 2.91, respectively. The results indicated that the train could

**Table 6** The  $\Delta\lambda_i$  corresponding to different sample sizes (PGA=0.2)

Characteristic parameter	Category	Sample size				
		20 (%)	40 (%)	60 (%)	80 (%)	100 (%)
Sample mean	Maximum bending moment of pier	3.6	0.6	-0.8	-0.7	0.4
	Maximum shear force of pier	-1.5	-0.5	0.0	0.4	0.3
	Maximum deformation of bearing	-0.7	-0.2	0.0	0.0	-0.1
	Maximum deformation of sliding layer	1.2	1.0	0.6	1.0	0.2
	Maximum deformation of CA mortar layer	4.5	-0.8	-0.2	0.6	0.5
	Maximum deformation of fastener	4.5	-0.1	-0.2	0.6	0.5
Sample standard deviation	Maximum bending moment of pier	8.2	0.6	3.3	-2.9	0.0
	Maximum shear force of pier	64.3	-4.3	-2.1	0.9	-1.3
	Maximum deformation of bearing	16.9	8.3	-3.8	-2.4	-0.5
	Maximum deformation of sliding layer	8.6	15.3	3.0	5.4	1.2
	Maximum deformation of CA mortar layer	36.6	1.8	-4.2	6.6	0.9
	Maximum deformation of fastener	33.4	4.3	-4.5	5.2	0.4

significantly amplify the seismic response of structure. Accordingly, the train's influence should be taken into consideration in earthquake resistant design.

## 5 Simplified method for seismic calculation of structures

According to the current Chinese “Code for Seismic Design of Rail Engineering” (Ministry of Railways of People’s Republic of China, 2009), the earthquake resistance of bridge should be checked, and considering both operating conditions with and without trains is necessary, and the train is considered as the additional mass right above the beam. However, the structural response obtained through this simulation method showed greater deviations from the real situations (He et al. 2011; Kim and Kawatani, 2006; Kim et al. 2007). Besides, in terms of checking calculation on the earthquake resistance of the bridge-track system, considering the role of moving trains would greatly increase the computational difficulty and is difficult to realize in design calculation. Table 7 indicate that regarding uncertain earthquake, the seismic response ratio under the operating conditions with and without trains was generally kept in the interval of  $(\lambda_L, \lambda_U)$ . Therefore, when the demand range for seismic response under the operating condition with vehicles was approximately simplified as the product of vehicle-free seismic response and the interval of  $(\lambda_L, \lambda_U)$ , the randomness of earthquake motion can be fully considered, and the design workload can be reduced.

**Table 7** Interval for the influence levels of trains on index response

Parameter	Category	PGA (g)									
		0.04	0.08	0.12	0.16	0.20	0.24	0.28	0.32	0.36	0.40
$\lambda_L$	Maximum bending moment of pier	1.32	1.17	1.11	1.08	1.06	1.06	1.06	1.05	1.04	1.04
	Maximum shear force of pier	0.99	0.99	0.99	0.99	0.99	0.99	0.99	0.99	0.99	0.99
	Maximum deformation of bearing	0.99	0.99	0.99	0.99	0.99	0.99	0.99	0.99	0.99	0.99
	Maximum deformation of sliding layer	1.55	1.50	1.50	1.66	1.88	1.99	2.08	2.15	2.44	2.75
	Maximum deformation of CA mortar layer	1.87	1.85	1.85	1.96	2.10	2.20	2.25	2.40	2.52	2.91
	Maximum deformation of fastener	1.86	1.85	1.84	1.94	2.06	2.21	2.25	2.34	2.54	2.86
	Maximum bending moment of pier	0.96	0.90	0.86	0.84	0.85	0.86	0.88	0.89	0.90	0.93
	Maximum shear force of pier	0.87	0.87	0.87	0.87	0.88	0.89	0.89	0.90	0.91	0.93
$\lambda_U$	Maximum deformation of bearing	0.84	0.85	0.85	0.85	0.85	0.86	0.88	0.89	0.90	0.91
	Maximum deformation of sliding layer	1.01	1.01	1.01	1.01	1.01	1.01	1.01	1.01	1.01	1.01
	Maximum deformation of CA mortar layer	1.01	1.01	1.05	1.07	1.09	1.13	1.18	1.16	1.09	1.01
	Maximum deformation of fastener	1.01	1.01	1.05	1.07	1.08	1.11	1.16	1.15	1.07	1.01

## 6 Conclusions

On the basis of considering the uncertainty of earthquake motion, the train–bridge coupled finite element model was established and verified through tests. The influence mechanism of trains on the structural response under the action of uncertain earthquake was analyzed, and the interval for the influence level of trains on structure response was counted. For the high-speed railway structures and trains described in Sect. 2, this study has the following conclusions:

1. When the PGA is smaller, the eccentric effect caused by moving trains has a significant influence on the bending moment of pier, and the influence of eccentric effect decreases with increasing PGA.
2. Under the action of earthquake, the presence of moving trains decreases the response of the pier and bearing and increases the response of the track structure, because the self deformation effect of the train and the interlayer deformation effect of the track structure caused by train inertia increase the dissipation of seismic energy. The change in the train speed does not significantly affect the seismic response of structures.
3. With increasing PGA, the influence of trains on the maximum deformation of sliding layer, mortar layer, and fastener increases, because the increase in PGA increases the force of trains on track structure; the influence of trains on the maximum bending moment, and maximum shear force of the pier and the maximum deformation of bearing gradually decreases, and most of the seismic energy is still dissipated by the pier and bearing under the action of strong earthquake.
4. For random earthquake motion, the seismic response ratio under the operating conditions with and without trains is basically maintained to be in the interval  $(\lambda_L, \lambda_U)$ . When the seismic response demand under the condition with trains is approximately simplified as the product of seismic response under the condition without trains and  $\lambda$ ,  $\lambda_U$ , the randomness of earthquake motion can be considered and the design workload can be reduced.

**Acknowledgements** This study was financially supported by the National Natural Science Foundation of China (52078487, 51778630 and U1934207) and the Hunan Innovative Provincial Construction Project (2019RS3009).

### Declaration

**Conflict of interest** The authors declare that they have no known competing financial interest or personal relationships that could have appeared to influence the work reported in this paper.

## References

- Chen L, Zhang N, Jiang L, Zeng Z, Chen G, Guo W (2014) Near-fault directivity pulse-like ground motion effect on high-speed railway bridge. *J Cent South Univ* 21(6):2425–2436. <https://doi.org/10.1007/s11771-014-2196-9>
- Fan B, Zhang Y, Ruan D (2014) Vibration analysis of bridge structure under moving train load and earthquake action. In: 3rd international conference on civil engineering and transportation (ICCET 2013), pp 1266–1269

- Feng Y, Jiang L, Zhou W, Han J, Zhang Y, Nie L, Tan Z, Liu X (2020) Experimental investigation on shear steel bars in CRTS II slab ballastless track under low-cyclic reciprocating load. *Constr Build Mater* 255(UNSP 119425). <https://doi.org/10.1016/j.conbuildmat.2020.119425>
- Gao X, Duan P, Qian H (2020) Dynamic response analysis of long-span continuous bridge considering the effect of train speeds and earthquakes. *Int J Struct Stab Dyn* 20(6):1–23. <https://doi.org/10.1142/S0219455420400131>
- Gong W, Zhu Z, Liu Y, Liu R, Tang Y, Jiang L (2020) Running safety assessment of a train traversing a three-tower cable-stayed bridge under spatially varying ground motion. *Railw Eng Sci* 28(2):184–198. <https://doi.org/10.1007/s40534-020-00209-8>
- He X, Kawatani M, Hayashikawa T, Matsumoto T (2011) Numerical analysis on seismic response of Shinkansen bridge–train interaction system under moderate earthquakes. *Earthq Eng Eng Vib* 10(1):85–97. <https://doi.org/10.1007/s11803-011-0049-1>
- Jarque CM (2011) *International encyclopedia of statistical science*. Springer, Berlin
- Jiang L, He W, Wei B, Wang Z, Li S (2019) The shear pin strength of friction pendulum bearings (FPB) in simply supported railway bridges. *Bull Earthq Eng* 17(11):6109–6139. <https://doi.org/10.1007/s10518-019-00698-x>
- Jiang L, Zhang Y, Feng Y, Zhou W, Tan Z (2020) Simplified calculation modeling method of multi-span bridges on high-speed railways under earthquake condition. *Bull Earthq Eng* 18:303–2328. <https://doi.org/10.1007/s10518-019-00779-x>
- Kang X, Jiang L, Bai Y, Caprani CC (2017) Seismic damage evaluation of high-speed railway bridge components under different intensities of earthquake excitations. *Eng Struct* 152:116–128. <https://doi.org/10.1016/j.engstruct.2017.08.057>
- Kim C, Kawatani M (2006) Effect of train dynamics on seismic response of steel monorail bridges under moderate ground motion. *Earthq Eng Struct Dyn* 35(10):1225–1245. <https://doi.org/10.1002/eqe.580>
- Kim C, Kawatani M, Lee C (2007) Seismic response of a monorail bridge incorporating train–bridge interaction. *Struct Eng Mech* 26(2):111–126. <https://doi.org/10.12989/sem.2007.26.2.111>
- Lee CH, Kim CW, Kawatani M, Nishimura N, Kamizono T (2005) Dynamic response analysis of monorail bridges under moving trains and riding comfort of trains. *Eng Struct* 27(14):1999–2013. <https://doi.org/10.1016/j.engstruct.2005.06.014>
- Liu Z, Jiang H, Zhang LF, Guo E D (2018) Natural vibration characteristics and seismic response analysis of train–bridge coupling system in high-speed railway. In: *International conference on experimental vibration analysis for civil engineering structures (EVACES)*, pp 831–838
- MRPRC (Ministry of Railways of People’s Republic of China) (2009) *Code for seismic design of railway engineering (in Chinese)* (GB50111-2006). China Planning Press, China
- Mu D, Gwon S, Choi D (2016) Dynamic responses of a cable-stayed bridge under a high speed train with random track irregularities and a vertical seismic load. *Int J Steel Struct* 16(4):1339–1354. <https://doi.org/10.1007/s13296-016-0104-x>
- Tondini N, Stojadinovic B (2012) Probabilistic seismic demand model for curved reinforced concrete bridges. *Bull Earthq Eng* 10(5):1455–1479. <https://doi.org/10.1007/s10518-012-9362-y>
- Wang H, Ding G, Tang H, Chen L (2011) *International conference on information engineering for mechanics and materials (ICIMM 2011)*, pp 566–570
- Wei B, Yang T, Jiang L, He X (2018) Effects of friction-based fixed bearings on the seismic vulnerability of a high-speed railway continuous bridge. *Adv Struct Eng* 21(5):643–657. <https://doi.org/10.1177/1369433217726894>
- Xia H, Han Y, Zhang N, Guo W (2006) Dynamic analysis of train–bridge system subjected to non-uniform seismic excitations. *Earthq Eng Struct Dyn* 35(12):1563–1579. <https://doi.org/10.1002/eqe.594>
- Xu L, Zhai W (2017) Stochastic analysis model for vehicle–track coupled systems subject to earthquakes and track random irregularities. *J Sound Vib* 407:209–225. <https://doi.org/10.1016/j.jsv.2017.06.030>
- Yan B, Liu S, Pu H, Dai G, Cai X (2017) Elastic-plastic seismic response of CRTS II slab ballastless track system on high-speed railway bridges. *Sci China Technol Sci* 60(6):865–871. <https://doi.org/10.1007/s11431-016-0222-6>
- Yu J, Jiang L, Zhou W, Liu X, Lai Z, Feng Y (2020) Study on the dynamic response correction factor of a coupled high-speed train–track–bridge system under near-fault earthquakes. *Mech Based Des Struct*. <https://doi.org/10.1080/15397734.2020.1803753>
- Zhai W, Liu P, Lin J, Wang K (2015) Experimental investigation on vibration behaviour of a CRH train at speed of 350 km/h. *Int J Rail Transp* 3(1):1–16. <https://doi.org/10.1080/23248378.2014.992819>
- Zhang ZC, Lin JH, Zhang YH, Zhao Y, Howson WP, Williams FW (2010b) Non-stationary random vibration analysis for train bridge systems subjected to horizontal earthquakes. *Eng Struct* 32(11):3571–3582. <https://doi.org/10.1016/j.engstruct.2010.08.001>

- Zhang N, Xia H, De Roeck G (2010a) Dynamic analysis of a train–bridge system under multi-support seismic excitations. *J Mech Sci Technol* 24(11):2181–2188. <https://doi.org/10.1007/s12206-010-0812-7>
- Zhang Z, Zhang Y, Lin J, Zhao Y, Howson WP, Williams FW (2011b) Random vibration of a train traversing a bridge subjected to traveling seismic waves. *Eng Struct* 33(12):3546–3558. <https://doi.org/10.1016/j.engstruct.2011.07.018>
- Zhang C, Zhong T, Chen K, Gong Y (2011) Study on the effects of train live loads on isolated and non-isolated simply supported railway bridges. In: *International conference on intelligent structure and vibration control (ISVC 2011)*, pp 100–104

**Publisher's Note** Springer Nature remains neutral with regard to jurisdictional claims in published maps and institutional affiliations.